CHINESE JOURNAL OF PHYSICS VOL. 37, NO. 4 AUGUST 1999

Dynamic Pulse Buildup in Continuous-Wave Passively Mode-Locked Picosecond Ti: Sapphire/DDI and Ti: Sapphire/IR140 Lasers

Ci-Ling Pan, Nen-Wen Pu, and Jia-Min Shieh
Institute of Electro-optical Engineering, National Chiao Tung University, Hsinchu, Taiwan 300, R.O.C.

(Received February 23, 1999)

We have studied both theoretically and experimentally the buildup of mode-locked pulses out of noise in continuous wave (cw) passively mode-locked Ti: sapphire lasers with DDI and IR140 dye saturable absorbers, which have significantly different optical properties. The evolution of the laser output from cw, to partial mode-locking, to complete mode-locking was investigated experimentally by measuring the contrast ratio of transient autocorrelation trace, the second-harmonic-generation (SHG) conversion efficiency, the fractional energy, optical and radio frequency (RF) spectra at consecutive delay times using the time-gating technique. Theoretically, we have simulated the pulse buildup numerically by adopting the two-level model for the saturable absorber. The experimental results are in good agreement with the predictions of numerical simulation.

PACS.42.55.Rz– Doped-insulator lasers and other solid state lasers.
PACS. 42.60.Fc– Modulation, tuning, and mode locking.

I. Introduction

The solid-state nature, high saturation power, excellent thermal, mechanical and optical properties, as well as broad bandwidth of the Ti: sapphire crystal have allowed it to become one of the most important laser materials for the generation and amplification of ultra-short optical pulses [1]. In the past decade: various mode-locking methods, some of them proposed and demonstrated for the first time, e.g., Kerr-lens mode-locking (KLM) [2], additive pulse mode-locking (APM) [3], and resonant passive mode-locking (RPM) [4], have been reported for the Ti: sapphire laser. Among them, passive mode locking using organic dye solutions as the saturable absorber has proven to be an easy and reliable way to generate picosecond (ps) or femtosecond (fs) light pulses [5]. Much effort has been devoted to the study of the pulse-forming dynamics and the effect of dyes in passively mode-locked Ti: sapphire lasers [6-9]. Our group [6] and Sarukura and Ishida [7] investigated the buildup dynamics of passively mode-locked Ti: sapphire lasers with DDI ($C_{27}H_{27}N_2I$ or 1,1'-Diathyl-2, 2'-dicarbocyanine Iodide) and HITCI (1,1',3,3,3',3'-Hexamethylindotricarbocyanine Iodide) dye jets as saturable absorbers respectively. Further, we showed that the pulse widths and the spectra of steady-state femtosecond pulses generated by the Ti: sapphire/DDI lasers were not affected by the concentration of the DDI jet, whereas those of picosecond pulses were [8]. This implies that nonlinear pulse shortening forces such as Kerr-lens effect and

self-phase modulation are dominant for femtosecond pulses but not picosecond pulses. In related work, Wang et al. [9] determined the self-starting threshold of the mode-locked Ti: sapphire/dye laser by varying the concentration of the intracavity dilute dye saturable absorber that starts the mode locking.

It is important to study the early startup stage of mode locking: which is the key to the understanding of physical mechanisms for pulse formation in the laser. Recently, we have improved the time-gating technique [10], which allows us to observe the evolution of laser output from cw all the way to complete mode-locked picosecond pulses. Transient autocorrelation traces and spectra can be measured. Three experimental parameters derived from the transient autocorrelation trace, i.e., the inverse contrast ratio, the second harmonic generation (SHG) conversion efficiency, and the fractional energy were found to be useful parameters in characterizing the degree of mode-locking of the laser during the pulse buildup. In this article, we review this experimental procedure in some detail. It is also shown that a two-level model for the saturable absorber can predict many of the features of pulse forming dynamics of the cw passively mode-locked Ti: sapphire laser with intracavity dye saturable absorbers. This is verified for two organic dyes: DDI and IR140 ($C_{39}H_{34}N_3O_4S_2Cl_3$) with significantly different characteristics, e. g., excited state lifetime and absorption cross-section.

II. Theoretical model and numerical simulation results

The primary pulse shortening mechanisms in passively mode-locked Ti: sapphire lasers with intracavity saturable absorbers but without dispersion-compensating prisms are saturable absorption and Kerr-lens-mode-locking (KLM). The effects of these two mechanisms on mode locking have been discussed and analyzed in many articles [11-12]. Most of the authors perform their analyses under the assumption that a well-defined single pulse has already formed [9, 13]. **This** is, however, not the case in the start-up stage of mode locking. Multiple pulses, pulses with complex structure, and pulses with cw background are very common in this stage. How the perfect picosecond single pulse grows out of cw noises is the central theme of the present study. Since the peak intensity of the laser output is relatively small in this stage, the nonlinear effects in the Ti: sapphire crystal such as self-phase modulation (SPM) and KLM can be neglected. In addition, gain saturation effect is insignificant in the Ti: sapphire crystal due to its high saturation intensity. Therefore, we are able to focus on the role of saturable absorber dyes played in mode locking. This is justified for the picosecond laser cavity considered in this work. The simplest model that can be used for describing the behavior of a saturable absorber is the two-level system. Let represents the absorbing population difference between lower and upper levels, the rate equation can be written as

$$\frac{d}{dt}\Delta N(t) = -\frac{2\sigma_a I(t)}{h\nu A_a}\Delta N(t) - \frac{\Delta N(t)}{\tau_a} + \frac{\Delta N_e}{\tau_a}, \tag{1}$$

where $h\nu$ and $I(t)$ are the photon energy and the light intensity of incident beam, respectively. The absorbing population difference under thermal equilibrium with 1(t) = **0** is given by AN,. A, is the beam area on the absorber. τ_a, σ_a are the excited state relaxation time and the absorption cross-section of saturable absorber, respectively. In the small signal

case, the relation between input and output intensities of laser beam through the saturable absorber: is given by

$$I_{out}(t) = I_{in}(t)\exp[-\sigma_a \cdot \Delta N(t) \cdot d_a], \tag{2}$$

where d_a is the path length of the Brewster-angled saturable absorber jet. The exponential term in Eq. (2) is just the transmittance of the saturable absorber.

$$T(t) = \exp[-\sigma_a \cdot \text{AN(t)} \ . \ d_a]. \tag{3}$$

At room temperature, AN, is approximately equal to the number of dye molecules per unit volume. In this work, the concentrations (in molar fractions) of DDI and IR140 dye jets are 3×10^{-4} M and 6×10^{-6} M, respectively. These correspond to the same linear absorption per pass, 1.5%. For DDI, $\sigma_a = 8 \times 10^{-18}$ cm^2[14] and τ_a = 30 ps [15]; for IR140, $\sigma_a = 4 \times 10^{-16}$ cm^2[14] and τ_a = 165 ps [15]. These and other relevant parameters of DDI and IR140 are summarized in Table I. For our laser system A, = 8×10^{-7} cm^2, and d_a = 100 μm. These were determined by measurements of the interference pattern of reflected beams from the dye jet. We assume the total laser energy in the cavity was maintained at 150 nJ. This is equivalent to an average output power of 600 mW. The Runge-Kutta-Fehlberg method [16] was employed to solve Eq. (1) for AN(t). We assumed that the initial laser intensity $I_{in}(t)$ consisted of purely cw noises with randomly phased longitudinal modes. Substituting $I_{in}(t)$ and AN(t) into Eq. (2), we can evaluate the output intensity, $I_{out}(t)$, through the absorber. For each round trip, the laser light passes through the absorber dye jet twice. The effect of the gain medium with negligible gain saturation is taken into account by keeping the total intracavity energy a constant, i.e., 150 nJ.

Figure 1 and Fig. 2 show the calculated results for the evolution of AN(t) and I(t) for a picosecond Ti: sapphire/DDI laser. In order to compare the prediction of the model with the experimental results, we have also computed the evolution of the normalized autocorrelation trace, $\Gamma(\tau)$. (See Fig. 3) It is defined as $\Gamma(n,\tau) = 2G^{(2)}(\tau)/G^{(2)}(0)$, where n is the delay in round trips with respect to the laser onset. τ is the relative delay between the two arms of the background-free second harmonic intensity autocorrelator. $G^{(2)}(\tau)$ is

TABLE I. Optical properties of the saturable absorber dyes, DDI and IR140. The working concentration was chosen such that the linear absorbances of the two dyes are the same.

Staturable Absorber Dye	Peak Absorption Wavelength λ_{max} (nm)	Absorption Cross-Section @λ = 770 nm	Excited-State Lifetime (ps)	Saturation Intensity (Mw/cm^2)	Working Concentration (M)
DDI	710	8×10^{-18}	30	1080	3×10^{-4}
IR140	810	4×10^{-16}	165	4	6×10^{-6}

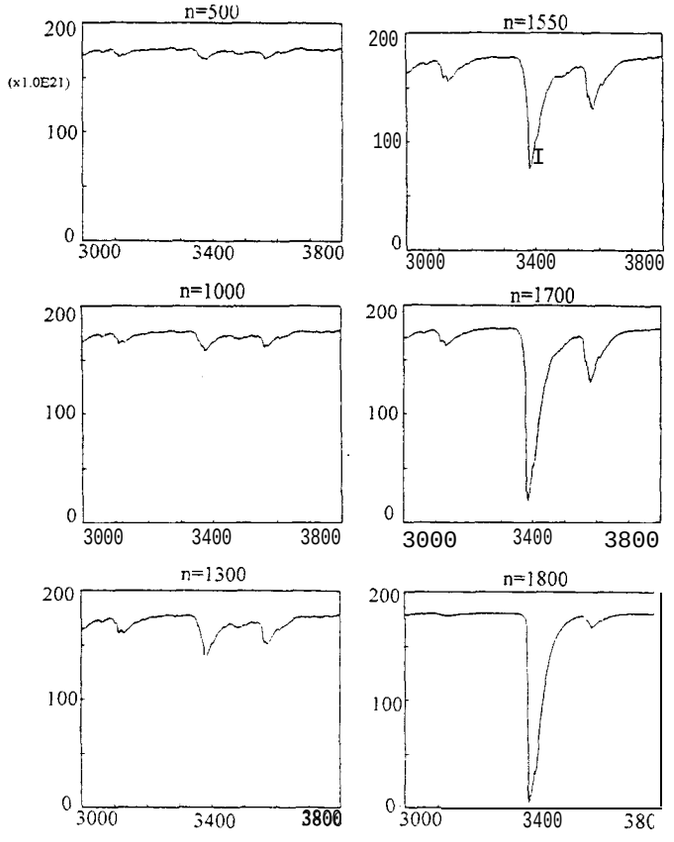

FIG. 1. Numerical simulation results for the evolution of AN(t) for a picosecond Ti: sapphire/DDI laser at a delay of n round trips from the laser onset (AN, = 1.8 x $10^{23}\mathrm{m}^{-3}$). The vertical axes are in units of $10^{21}\mathrm{m}^{-3}$. The horizontal axes are in units of picoseconds.

the intensity autocorrelation function given by $G^{(2)}(\tau) = \int_{-\infty}^{\infty} I(t)I(t+\tau)dt$. The maximum value of $\Gamma(\tau)$ is normalized to 2, according to the conventional definition. The corresponding results for IR140 case are shown in Fig. 4 through 6. Examining Fig. 1 through 6, we can discern some apparent differences between the two cases:

(1) It is much easier to saturate IR140 than DDI, as shown in the evolution of AN(t). For IR140, saturation will occur even in the cw stage. This is because the saturation intensity I_s of IR140 is two orders of magnitude smaller than that of DDI (see Table I).

(2) The recovery time for IR140 after saturation is obviously longer than that of DDI. This is due to the longer excited-state relaxation time for IR140.

(3) In the early stage, at least for the first 1000 round trips after the laser onset, IR140 provides stronger selective absorption than DDI. This is also due to the low saturation

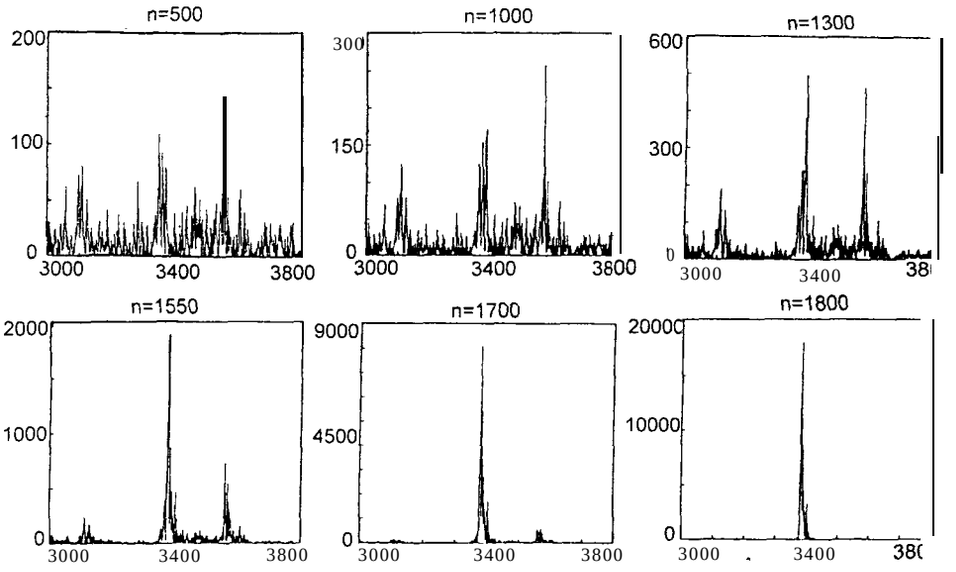

FIG. 2. Numerical simulation results for the evolution of the intracavity peak power, I(t) for a picosecond Ti: sapphire/DDI laser at a delay of n round trips from the laser onset. The vertical axes are in Watts. The horizontal axes are in units of picoseconds.

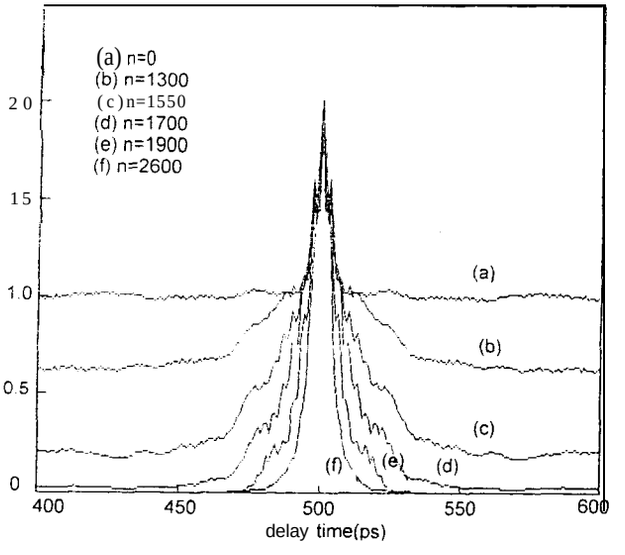

FIG. 3. Numerical simulation results for the evolution of the normalized autocorrelation traces, $\Gamma(\tau)$, for a picosecond Ti: sapphire/DDI laser at a delay of n round trips from $n = 0$ to n = 2600. The horizontal axis is in unit of picoseconds.

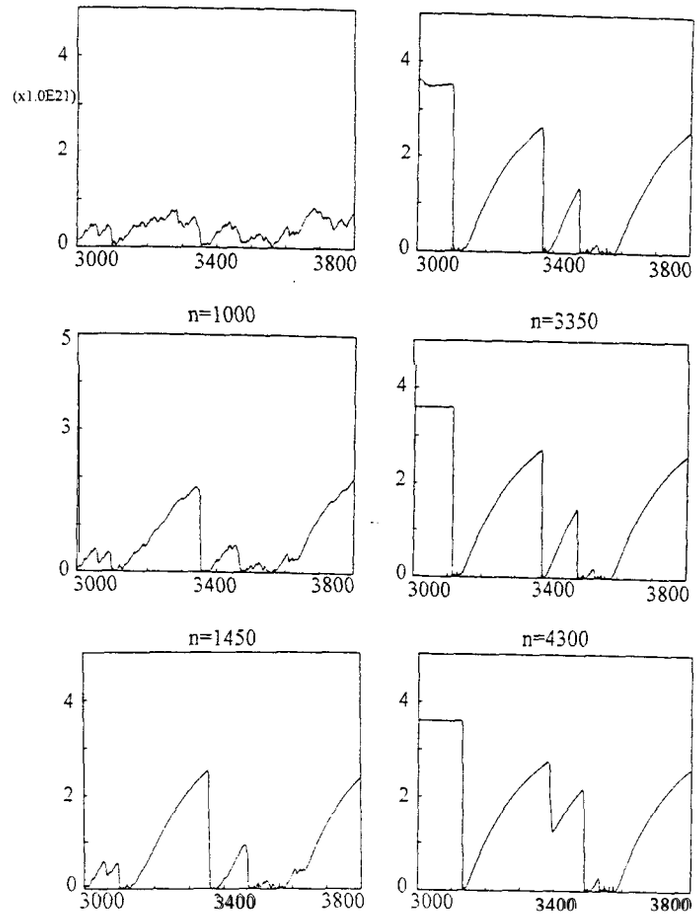

FIG. 4. Numerical simulation results for the evolution of $\Delta N(t)$ for a picosecond Ti: sapphire/IR140 laser at a delay of n round trips from the laser onset ($\Delta N_e = 3.6 \times 10^{21} m^{-3}$). The vertical axes are in units of $10^{21} m^{-3}$. The horizontal axes are in units of picoseconds.

intensity of IR140 (see Table I). It is well known that the discrimination of low-intensity noise bursts from high-intensity ones is the primary mechanism for pulse formation [17]. In the cw stage, when all the noise bursts are relatively small, an absorber with lower saturation intensity will more easily pick the larger noise bursts out of the average. Compare Fig. 2 with Fig. 4, we find the pulse forming speed of the Ti: Sapphire/DDI laser is much faster than that of the Ti: Sapphire/IR140 laser after 1500 round trips. A "pulse" is nearly shaped for the Ti: Sapphire/DDI laser at about 1900 round trips. On the other hand, it takes more than 5000 round trips for the Ti: Sapphire/IR140 laser to reach the same state, which is about 3 times as long. This is also due to the low saturation intensity of IR140, as well as the longer relaxation time. It is so easily saturated and takes such a long time to recover that hardly any

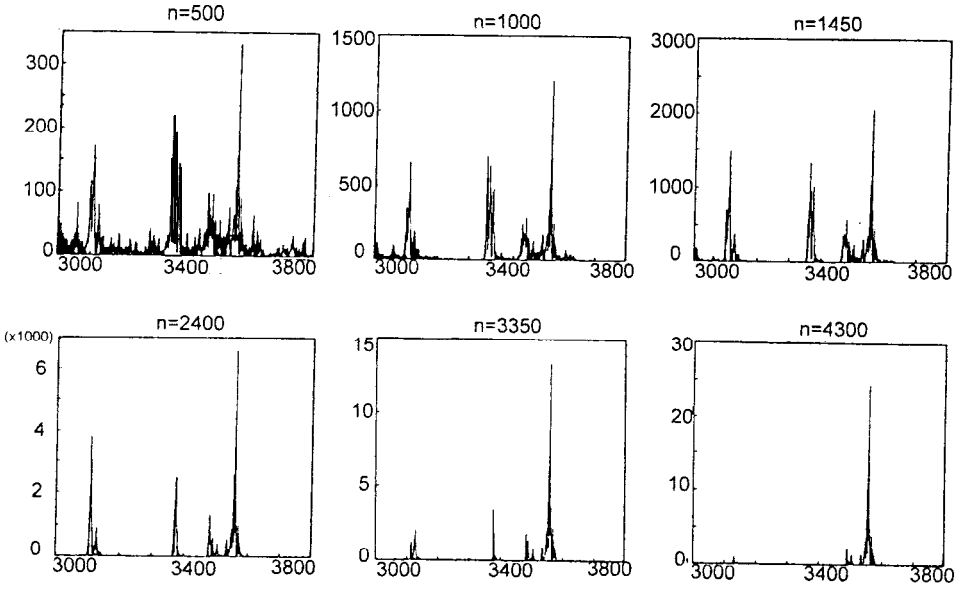

FIG. 5. Numerical simulation results for the evolution of the peak intracavity power, I(t), for a picosecond Ti: sapphire/IR140 laser at a delay of n round trips from the laser onset. The vertical axes are in Watts. The horizontal axes are in units of picoseconds.

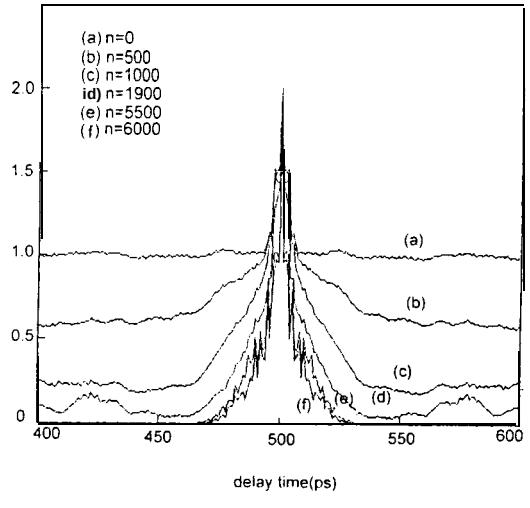

FIG. 6. Numerical simulation results for the evolution of the normalized autocorrelation traces, $\Gamma(\tau)$, for a picosecond Ti: sapphire/IR140 laser at a delay of n round trips from $n = 0$ to n = 6000. The horizontal axis is in unit of picoseconds.

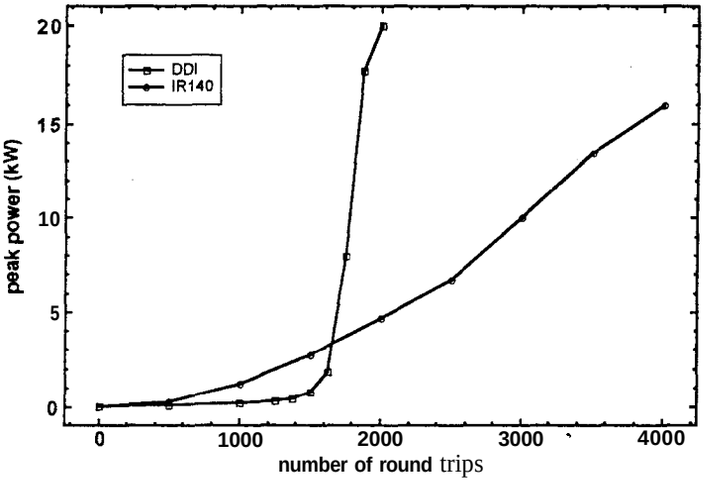

FIG. 7. Numerical simulations of the evolutions of the peak intracavity intensity of the largest noise burst for picosecond Ti: sapphire/DDI and Ti: sapphire/IR140 lasers as a function of the delay time in number of round trips.

significant suppression of the undesired noise bursts can be achieved. Compared to the Ti: sapphire/DDI laser, there are more clusters of undesired noise bursts apart from the primary one in a Ti: sapphire/IR140 laser at the same stage. Figure 7 illustrates this phenomenon by tracing the evolution of peak intracavity intensity for the largest noise burst in each case.

We have also simulated the pulse evolution of the passively mode-locked Ti: Sapphire/DDI laser for various dye concentrations. This is shown in Fig. 8. The buildup time for the formation of mode-locked pulses is apparently an exponential function of dye concentration. This can be easily understood from the exponential form of transmission function of dye given in Eq. (4). Based on the above numerical results, we can make the following observations about the role of the dye saturable absorber in the pulse forming process of passively mode-locked Ti: sapphire lasers without dispersion-compensating prisms:

(1) The dyes are not merely starters of mode locking. Picosecond single pulses can grow out of the cw signals by the help of the saturable absorber dyes without the presence of KLM.

(2) The pulse forming dynamics down to the ps regime depends mostly on the dye parameters e.g., τ_a, and σ_a.

(3) A plausible physical picture of mode locking in these lasers is as follows: In the beginning, thousands of randomly phased modes in the cavity interfere with each other. As a result, the cw laser output is described by the so-called Gaussian noises. With the presence of the saturable absorber dye, the strongest noise bursts are selected and amplified, while the others are gradually suppressed. Finally, a primary cluster of noise burst is formed which eventually evolves into the single pulse.

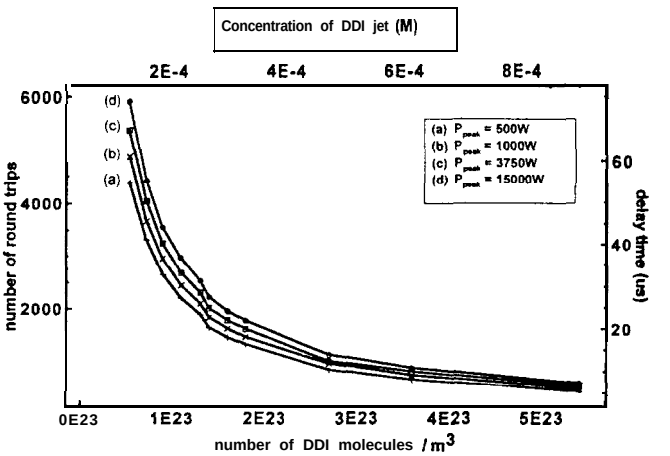

FIG. 8. Numerical simulations of the effect of the dye concentration on the buildup time of the intracavity peak power of the largest noise burst to (a) 500 W, (b) 1000 W, (c) 3750 W, (d) 15000 W in a picosecond passively mode-locked Ti: Sapphire/DDI laser.

III. Experimental methods

A block diagram of the experimental setup is shown in Fig. 9. The configuration of ps passively mode-locked Ti: sapphire laser is shown in the inset of Fig. 9. It employed an 8-mm Ti: sapphire crystal in a six-mirror linear astigmatically compensated cavity. The Ti: sapphire laser was aligned such that it would not self-start without the saturable dye jet. That is, the Kerr-lens strength was weak. The lasing wavelength was set at $\lambda = 770$ nm by a 0.5-mm-thick birefringent filter. Self-starting, sustaining and stable mode-locked pulses were achieved for DDI concentrations in the range of 2 x 10^{-5} to 10^{-3} M. Pumped by an all-lines 6-W cw argon-ion laser, the Ti: sapphire/DDI and Ti: Sapphire/IR140 lasers routinely generate steady-state pulses with duration's of 5ps and 10ps, respectively. With 5% output coupling, the average output powers were 600 mW at 79.4 MHz. For the investigation of the dynamics of pulse formation in our laser, the cw argon-ion laser was mechanically chopped to produce 500-Hz square pulses with a FWHM of lms and a rise time of 2 μs. The output was divided into three beams. The first beam was detected by a fast photodetector for a real-time display of the pulse train on the oscilloscope. The second beam was directly detected by a gatable photomultiplier tube, gated by 1-ms pulses delayed with respect to the onset of the laser. The output was sent to a RF spectrum analyzer that monitors the transient beat notes. The third beam was fed to a non-collinear autocorrelator or a monochromator and detected by a photomultiplier tube. A boxcar integrator with a 50-ns gate then selected four pulses in the window at a given delay time and averaged the signal. By delaying the gate with respect to the chopped pumping signal, we can sample the transient temporal and spectral behavior of the output of the Ti: sapphire laser at consecutive moments in the evolution process.

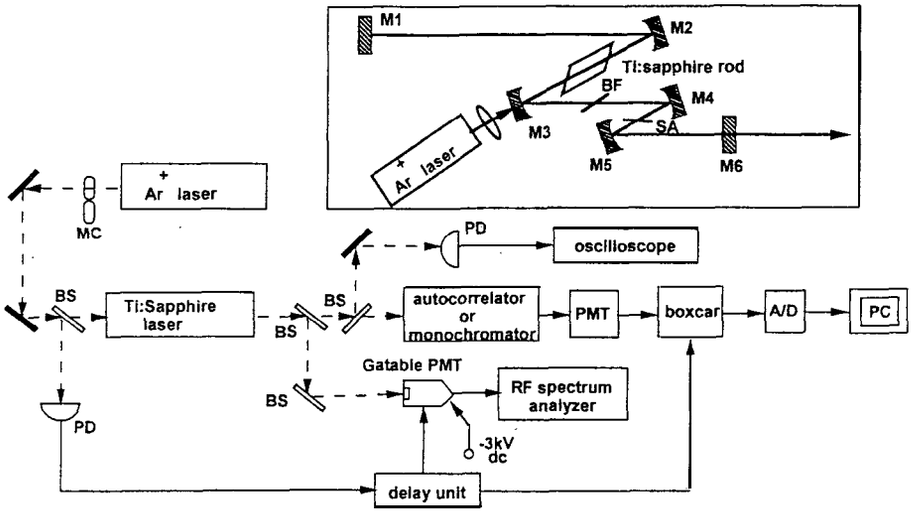

FIG. 9. Block diagram of the experimental arrangement: MC, mechanical chopper; BS's, beam splitters; PD's, photodetectors; PMT's, photomultiplier tubes; PC, personal computer: A/D, analog-to-digital converter. The inset shows the configuration of the passively mode-locked picosecond Ti: sapphire/dye laser; SA, saturable absorber, BF, birefringent filter; Ml íV M6, mirrors.

IV. Experimental results and discussions

For various concentration of DDI, the pulse formation time: the steady-state buildup time, the steady-state pulse width, and the steady-state time-bandwidth product are summarized in Table II. It is interesting that all these quantities are exponentially dependent on the concentration. The exponential form of transmission function of dye can also explain this. It is in good agreement with the simulation results as well. For the data presented below, the concentrations of DDI and IR140 are fixed at the values given in Table I.

From the real-time oscilloscope trace (see Fig. 10), we observed that the chopped laser output exhibited relaxation oscillation at 200 kHz during the first 15 μs after the laser onset. Afterwards, a pulse train appeared and soon became stable at about 45 μs for the Ti: sapphire/DDI laser, and 150 μs for the Ti: sapphire/IR140 laser. Relaxation oscillation is caused by the interplay of population inversion and stimulated emission. Because gain saturation is not an important pulse-shaping mechanism in solid-state lasers, we do not expect relaxation oscillation to affect the starting dynamics of the Ti: sapphire/DDI or /IR140 laser.

The normalized background-free intensity autocorrelation traces are plotted as a function of the delay time in Fig. 11 for the Ti: sapphire/DDI laser and Fig. 12 for the Ti: sapphire/IR140 laser, respectively. Zero delay time was chosen to coincide with the first relaxation-oscillation peak. Curve (a) in each of the above two figures is a typical autocorrelation trace for a randomly phased cw laser. The baseline of the trace is at unity.

TABLE II. The effect of DDI concentration on the pulse forming dynamics of the picosecond Ti: sapphire/DDI laser.

Dye Concentration (10^{-4}M)	Linear Loss (%)	Pulse Forming Time (round trips)	Steady-State Buildup Time (round trips)	Steady-State Pulse Width (ps)	Pulse Width BW Product $\Delta\nu\Delta\tau$
6.0	3	1200	3600	- 2	$\sim$ 2.0
3.0	1.5	1300	4000	- 5	$\sim$ 4.0
1.25	0.7	3600	6400	$\sim$ 8.5	$\sim$ 8.0
0.84	0.4	11900	20000	$\sim$ 12	$\sim$ 11

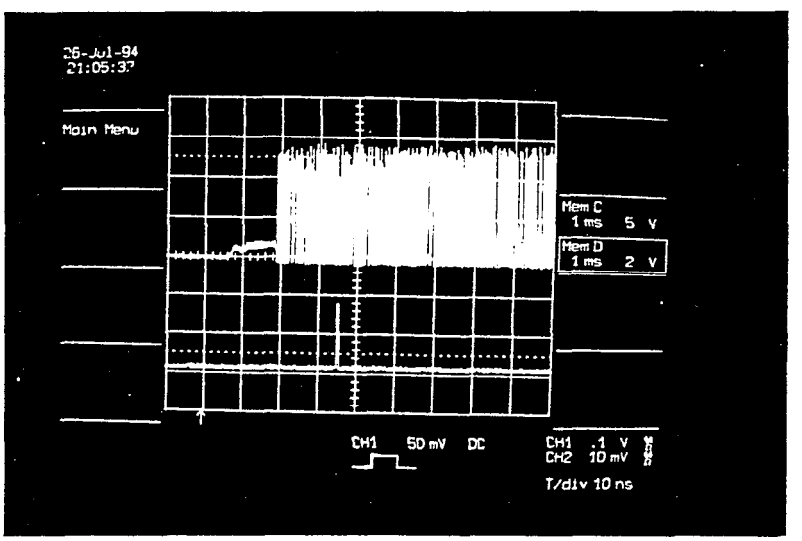

FIG. 10. Real-time display of the dynamics of pulse formation. The upper trace is the chopped argon-ion laser pump pulse. The lower trace shows the pulse train buildup in the Ti: sapphire/dye laser measured with a fast photodetector.

Fig. 11(a) exhibits a 9-ps-wide coherent spike. The coherent spike is due to a chaotic collection of picosecond fluctuations, not to well-defined picosecond pulse[18-20]. The width of this spike corresponds to the coherence time of the laser [18] and should be inversely proportional to the spectral bandwidth of the laser [18-19]. From this formula, we estimated that the corresponding bandwidth of the Ti: sapphire/DDI laser was about 2Å. This is in good agreement with our spectral measurements. (See Figs. 15 and 16) The secondary spikes located at approximately a 10-ps delay from the coherent spike peak were due to the

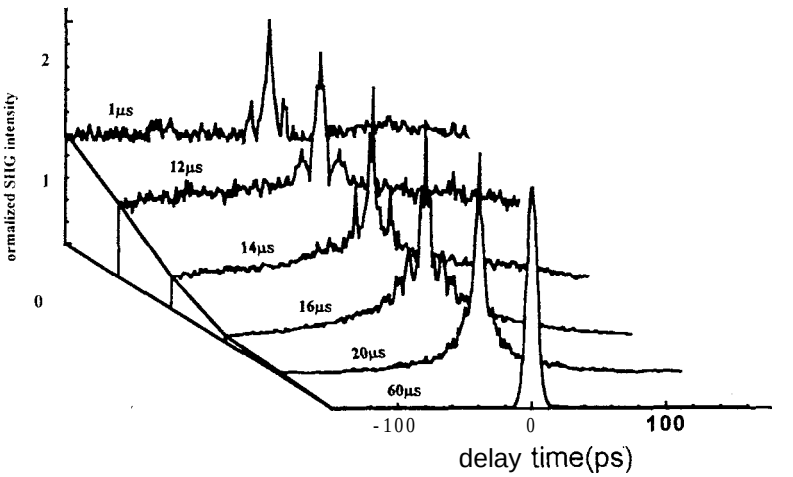

FIG. 11. Experimentally observed transient intensity autocorrelation traces of a picosecond Ti: sapphire / DDI laser at different delay times after the laser onset.

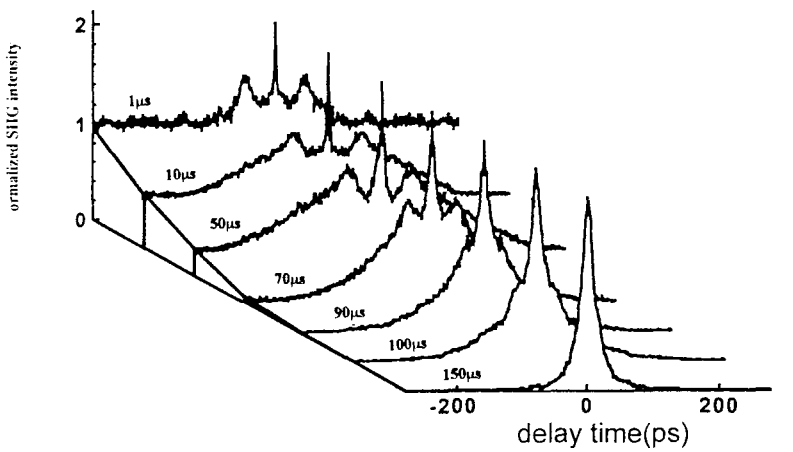

FIG. 12. Experimentally observed transient intensity autocorrelation traces of a picosecond Ti: sapphire/IR140 laser at different delay times after the laser onset.

mutual correlation between side clusters of longitudinal modes observed in our transient spectral measurements (See also Fig. 15 and 16). For the Ti: sapphire / DDI laser, an autocorrelation trace (trace (e) in Fig. 11) with negligible background was first observed at about 20 μs (or $\approx$ 1600 round trips). The baseline of trace (e) in Fig. 11 is nearly zero. The height and FWHM of the shoulder are 0.23 and 72 ps respectively. The distinction between the coherence spike and the shoulder is not apparent. The corresponding time for

the Ti: Sapphire/IR140 laser to reach this state is about 90 μs (or $\approx$ 7200 round trips) while the height and FWHM of the shoulder are 0.75 and 175 ps respectively. This trend is in good agreement with our theoretical prediction presented in Sec. 2.

In order to examine the buildup dynamics more quantitatively, we introduce the following parameters: First of all, we define the contrast ratio, R, as the peak-to-shoulder ratio of the autocorrelation trace, i.e., the local contrast ratio [20]. In the 1970's, many numerical calculations have been performed to simulate varying degrees of mode locking of the laser with the contrast ratio as an index [21-25]. R^{-1} is related to the contrast ratio in the two-photon fluorescence (TPF) case, $R_{TPF} = 3/(2R^{-1}+1)$, in the above studies [23]. The SHG conversion efficiency $\varepsilon^{(2)}$ and the fractional energy β were also found to be useful for characterizing the pulse formation process. The SHG conversion efficiency is defined as $\varepsilon^{(2)} = E_1^{(2)}/E_2^{(2)}$, where $E_1^{(2)}$ denotes the actual SHG energy generated and $E_2^{(2)}$ is the SHG energy that would have been generated by the fundamental wave of the same shape and of the same total energy but without background. Previously, Von der Linde [24] has pointed out $\varepsilon^{(2)}$ is insensitive to the pulse shape and is a very sensitive measure of the background level. The transient value of $\varepsilon^{(2)}$ was obtained by measuring the transient fundamental power, the SHG power, and the pulse width [26]:

$$\varepsilon^{(2)} = \frac{\tau_p(\bar{p}_\omega^{ss}/\bar{p}_\omega)^2}{\tau_p^{ss}(\bar{p}_{2\omega}^{ss}/p_{2\omega})}, \tag{4}$$

where $\tau_p, \bar{p}_\omega$, and $\bar{p}_{2\omega}$ are transient pulse width, fundamental power, and SHG power: respectively. The parameters, $\tau_p^{ss}, \bar{p}_\omega^{ss}, \bar{p}_{2\omega}^{ss}$ are corresponding steady-state values. The fractional energy β is defined as $\beta = \frac{E_p}{E_{total}}$, where E_p is the energy of the pulse and E_{total} is the energy of pulse with background. It can be calculated from the SHG conversion efficiency by using the relation [24]:

$$\varepsilon^{(2)} = \beta^2 \left[\sum_{\nu=0}^{2} v! \begin{pmatrix} 2 \\ \nu \end{pmatrix}^2 \left(\frac{\tau_p}{T}\right)^v \left(\frac{1}{\beta} - 1\right)^v \alpha_{2\nu} \right], \tag{5}$$

and

$$\alpha_{2\nu} = \left(\frac{1}{t_p}\right)^\nu \left\{ \frac{\left(\int_{-T_R/2}^{T_R/2} |V_p(t)|^2 dt \right)^\nu \left(\int_{-T_R/2}^{T_R/2} |V_p(t)|^{2(2-\nu)} dt \right)}{\left(\int_{-T_R/2}^{T_R/2} |V_p(t)|^4 dt \right)} \right\}, \tag{6}$$

where T_R, τ_p, V_p are respectively, the cavity round trip time, the pulse width, and the analytic signal associated with the optical field of the pulse envelope.

Let us examine the autocorrelation traces shown in Fig. 11 in some detail using the above parameters. During the first 10 μs, the contrast ratio remained nearly a constant, $R \approx 2$, or $R^{-1} \approx 0.5$. The laser behaved like a cw laser. As the circulating energy inside the cavity increased and saturated the absorber dye, the output of the Ti: sapphire laser became slightly modulated. In this stage (see curves (b) and (c) of Fig. 11), a very small degree of

interdependence among the phases of a few neighboring modes has been developed. Thus the value of R^{-1} gradually decreased, but an apparent pulse profile has yet appeared. At 16 μs ($\approx$ 1280 round trips): the autocorrelation trace displayed a low baseline, upon which was superposed a broad Lorentzian shoulder with a width τ_g of $\approx$ 155 ps and a normalized height of $\approx$ 0.3. The width of the central coherent spike remained unchanged throughout the buildup process up to this point. The width of the broad hill on which the spike rides, τ_g, is proportional to the duration of the burst of light with phase-locked modes [18], while the presence of the narrow central spike reveals the unclean appearance of the burst of light with numerous picosecond substructures on it [18-25]. At 20 μs($\approx$ 1600 round trips), we observed the first autocorrelation trace with negligible cw background in the whole buildup process, with a peak-to-shoulder contrast ration of $\approx$8.7 ($R^{-1}\approx$ 0.12), [curve (e) of Fig. 11]. The central portion of the trace has a two-sided exponential profile. This corresponds to 4.4 ps - wide primary pulse. The residual pedestal in the trace (assumed to be Lorentzian) has a width of $\sim$ 72 ps and a normalized height of $\sim$ 0.23. Further locking of modal phases manifested as increasing R until the steady state with practically infinite contrast ($R^{-1}\sim 0$) was reached. At a delay of 40 μs, a time-bandwidth product $\tau_p\Delta\nu\approx$ 0.5 was measured. This is close to the transform limit of Gaussian pulses (0.44). We note further that after 45 μs, the laser spectra broadened considerably due to the effect of self-phase modulation (SPM) [27]. The tine-bandwidth product eventually increased to $\sim$ 4, much greater than the transform limit. This implies the existence of significant chirp within the pulse. The steady-state pulse shape is Gaussian; with a FWHM pulse width of 5 ps. The steady-state pulse width for the Ti: sapphire/IR140 laser is $\sim$ 10 ps.

In Figs. 13 and 14, we display the inverse contrast ratio, R^{-1}, as a function of delay time (open squares) for Ti: sapphire/DDI and Ti: sapphire/IR140 lasers, respectively. Also shown in Figs. 13 and 14 are the SHG conversion efficiency $\varepsilon^{(2)}$ (filled circles) and the fractional energy β (open circles) as a function of the delay time. As we can see in Figs. 13 and 14, the parameters, R^{-1},$\varepsilon^{(2)}$, and β all exhibit apparent asymptotic behavior toward the steady state. Thus they are convenient for quantitatively characterizing different stages during the buildup of mode-locked pulses. In the cw regime, the contrast ratio, $R \sim 2$. or $R^{-1} \sim 0.5$, while $\varepsilon^{(2)}$ and β are nearly zero. When more and more longitudinal modes were locked with stronger phase interdependence, the value of R^{-1} began to decrease, while $\varepsilon^{(2)}$ and β increased. Further locking of modal phases manifested itself as increasing R or decreasing $\varepsilon^{(2)}$ or β until the steady state was reached. The steady-state pulse exhibited an autocorrelation trace with nearly zero background, practically infinite contrast ($R^{-1}\sim 0$) and 100% SHG conversion efficiency and fractional energy. Examining Fig. 14, we find that second harmonic signal for the Ti: sapphie/IR140 laser was observed very earlier but rose rather slowly during the buildup, while R^{-1} remains $\sim$ 0.5 until a delay of $\sim$70 μs. In contrast, a sharp decline of R^{-1} and subsequently rapid rise of $\varepsilon^{(2)}$ or β were observed for the Ti: sapphire/DDI laser after the fist 10 μs. Furthermore, the buildup time for the Ti: sapphire/DDI laser, which almost reached its steady state at 60 μs($\approx$ 4800 round trips). was much faster than the Ti: sapphie/IR140 laser (about 150 μs or 12000 round trips). These are consistent with the theoretical predictions presented in section 1. We note that the steady state pulse width for the Ti: sapphire/DDI laser (5 ps) was also significantly shorter than that of the Ti: sapphire/IR140 laser (10 ps). To calculate the steady-state pulse width, one has to include all kinds of broadening and shortening mechanisms and find

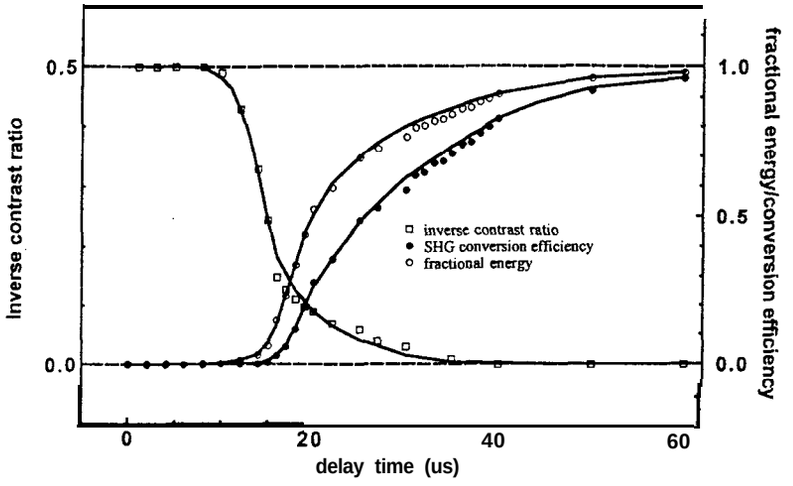

FIG. 13. The inverse contrast ratio, R^{-1} (open squares), SHG conversion efficiency $\varepsilon^{(2)}$ (filled circles) and the fractional energy β (open circles) as a function of the delay time for a picosecond Ti: sapphire/DDI laser.

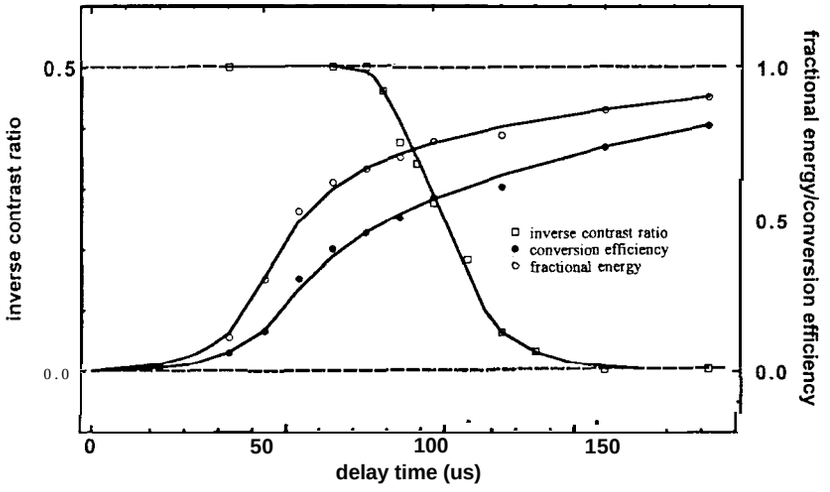

FIG. 14. The inverse contrast ratio, R^{-1} (open squares), SHG conversion efficiency $\varepsilon^{(2)}$ (filled circles) and the fractional energy β (open circles) as a function of the delay time for a picosecond Ti: sapphire/IR140 laser.

the balancing point for them. This is the subject of our forthcoming paper. Our simple model gives a rough estimate of the steady-state pulse, ~ 10 ps for both lasers. This is of the same order of magnitude as the experimental data.

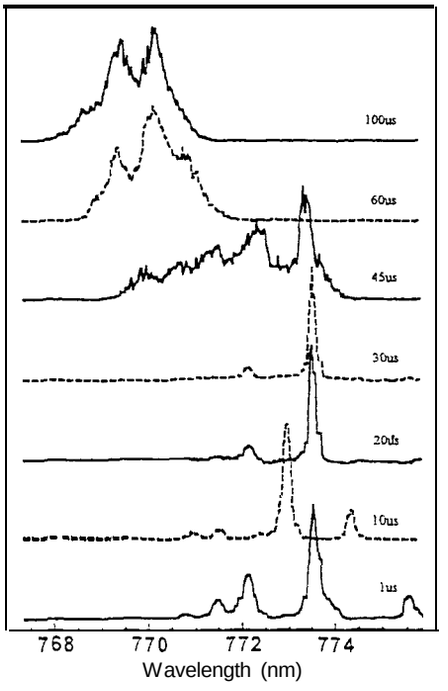

FIG. 15. The evolution of the optical spectra for the output of a picosecond Ti: sapphire / DDI laser during the pulse buildup.

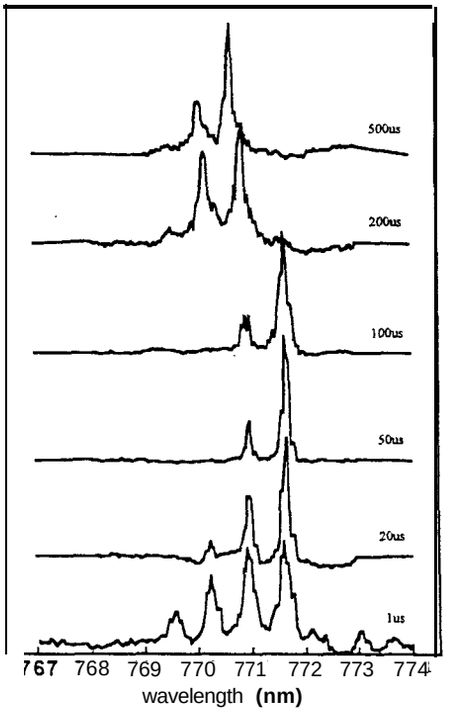

FIG. 16 The evolution of the optical spectra for the output of a picosecond Ti: sapphire/IR140 laser during the pulse buildup.

Fig. 15 and 16 show the evolution of optical spectra for the two cases. In the starting stage of both lasers, we observe spectral features separated by 0.7 nm. This was due to the etalon effect of the 500-mm-thick, Brewster-angled birefringent filter. We note that there was a spectral blue shift for the Ti: sapphire/DDI laser as it evolved to the steady state. This can be qualitatively explained by the shift of the net gain curve due to the saturation of DDI [6, 7]. The absorption peak of DDI dissolved in ethylene glycol is at 710 nm, whereas the gain peak of Ti: sapphire is at 800 nm. As DDI became saturated during the evolution, the net gain of the laser shifted to the blue. This phenomenon, however. was not observed in the Ti: sapphire/IR140 laser. It can be easily explained. Examining Fig. 4, we can see that the IR140 dye is highly saturated even at the beginning of the cw regime. There is no mechanism for the gain curve to shift throughout the evolution process. Also note that for the Ti: sapphire/DDI laser the spectra broadened considerably as the steady-state 5-ps pulse was formed (at a delay beyond $\sim 45\ \mu s$). This is manifestation of the nonlinear self-phase modulation (SPM) effect. Concurrently, the time-bandwidth product of the laser increased from 0.5 ($\tau_{delay} \approx 30 \sim 40\ \mu s$) to 4 ($\tau_{delay} \geq 60\ \mu s$), much greater than the transform limit. This implies the existence of significant chirp within the pulse.

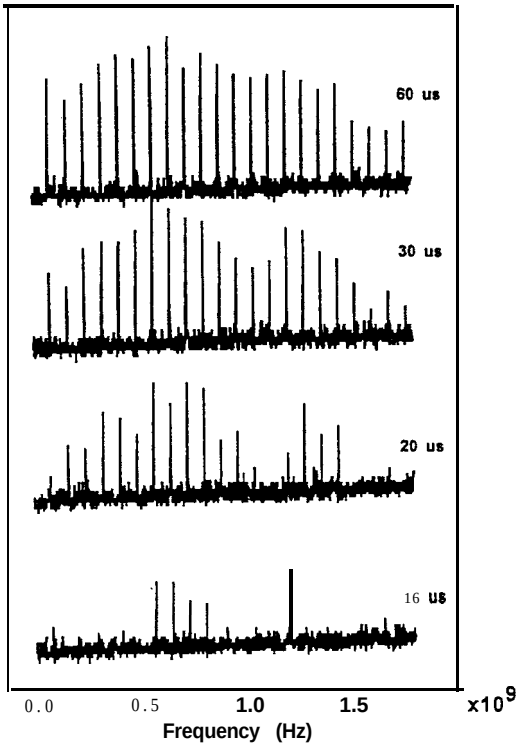

FIG. 17. The transient RF beat-note spectra for a picosecond Ti: sapphire/DDI laser during the pulse buildup.

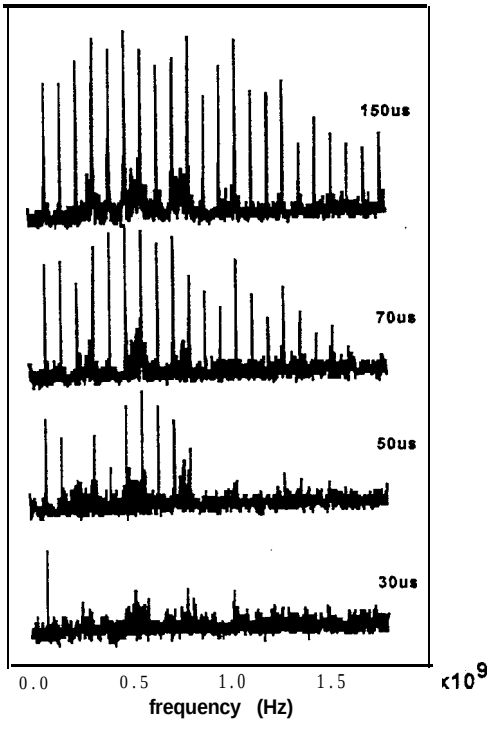

FIG. 18. The transient RF beat-note spectra for a picosecond Ti: sapphire/IR140 laser during the pulse buildup.

Comparing to the Ti: Sapphire/DDI laser; the spectral broadening of the Ti: sapphire/IR140 laser is much less pronounced. This is because its steady-state pulse duration is twice as long ($\sim$ 10 ps). As a result, the intracavity peak intensity is only half the value of the Ti: sapphire/DDI laser and hence less spectral broadening due to SPM.

We note that the pulse-evolution data correlate well with the transient optical spectra as well as the RF beat-note spectra shown in Fig. 17 and 18. For the latter, we found that some beat notes began to emerge as the mode locking proceed (at a delay time of 16 μs for DDI and 50 μs for IR140). The growth of these beat notes implies the increasing degree of interdependence between modal phases and therefore is an indication of the extent of mode locking. The steady-state RF beat-note spectra was observed at about 60 μs for the Ti: sapphire/DDI laser, and 150 μs for the Ti: sapphire/IR140 laser. These are also in good agreement with the observation of trends for the autocorrelation traces.

IV. Summary

In this article, we review in detail our theoretical and experimental studies of the entire build-up process of mode-locked pulses in cw passively mode-locked picosecond Ti:

sapphire lasers with intracavity dye saturable absorbers. We show that a two-level model of the saturable absorber dye is satisfactory for simulation of the pulse build-up process in these lasers. The evolution of laser output using two kinds of dyes with significantly different excited-state lifetimes and cross- sections, DDI and IR140, were presented. We found that, rather than serving as merely a starter of mode locking, the nonlinear absorption of dye is actually the most significant mechanism in a laser cavity without dispersion-compensating prisms and weak Kerr-lens strength. The mode-locking process depends on the dye parameters τ_a, I, and N_e. In the early, stage, IR140 provides stronger selective absorption than DDI for self-starting. On the other hand, the pulse forming speed of the Ti: Sapphire/DDI laser is much faster than that of the Ti: Sapphire/IR140 laser due to the low saturation intensity of IR140, as well as the longer relaxation time. By the help of the saturable absorber dyes, picosecond pulses can grow out of the cw noises without the presence of KLM.

Experimentally, we were able to examine the complete dynamic process of pulse formation from the cw stage to the steady state using the time-gating technique. Incomplete mode locking of various degrees that were determined quantitatively from the inverse contrast ratio of transient autocorrelation trace, the SHG conversion efficiency, and the fractional energy were observed. The comparison between the two different dyes DDI and IR140 being used as the saturable absorbers has been made. The corresponding transient RF beat notes spectra and the optical spectra are also consistent with the above measurements. The experimental results are in good agreement with the predictions of our numerical simulation.

Acknowledgments

This work was supported in part by the National Science Council of the Republic of China under various grants.

References

[1] K. Yamakawa *et al.*, Opt. Lett. 23, 525 (1998).
[2] L. Spinelli *et al.*, Dig. Conf. Lasers Electra-Opt., Washington, D. C., Opt. Soc. Amer., 1991, Paper CPDP7.
[3] J. Mark *et al.*, Opt. Lett. 14, 48 (1989).
[4] U. Keller, W. H. Knox, and H. Roskos, Opt. Lett. 15, 1377 (1990), H. A. Haus *et al.*, J. Opt. Soc. Am. B8, 1252 (1991).
[5] N. Sarukura and Y. Ishida, Opt Lett. 18, 888 (1992).
[6] J.-C. Kuo *et* al., Opt. Lett. 17, 334 (1992).
[7] N. Sarukura and Y. Ishida, Opt Lett. 17, 61 (1992).
[8] Ci-Ling Pan *et al.*, Opt. Lett. 17, 1444 (1992).
[9] Yuh-Fwu Chou *et al.*, Opt. Lett. 19, 566 (1994).
[10] N.-W. Pu *et al.*, Opt. Lett. 19, 566 (1994).
[11] H. A. Haus, J. Appl. Phys. 46, 3049 (1975).
[12] G. Cerullo, S. De Solvestri, and V. Magni, Opt. Lett. 19, 1040 (1994).
[13] Ferenc Krausz *et al.*, IEEE J. Quantum Electron. **QE-28, 2097 (1992).**
[14] P. Sperber *et al.*, Opt. Quantum Electron. 20, 395 (1988).

[15] F. Ganikhanov, J. -M. Shieh, and Ci-ling Pan, Optics Communications, 114, 289 (1995).
[16] L. Lapidus, and J. H. Seinfeld, in *Numerical solutions of ordinary differential equations* (New York: Academic, New York, 1971).
[17] S. L. Shapiro, *Ultrashort light pulses* (Topics in Appl. Phys., Vol. 18). (Berlin-New York: Springer-Verlag, 1997).
[18] D. J. Bradley, and G. H. C. New, Proc. IEEE 62, 313 (1974).
[19] H. A. Pike and M. Hercher, J. Appl. Phys. 41, 4562 (1970).
[20] M. A. Duguay, J. M. Hansen, and S. L. Shapiro, IEEE J. Quantum Electron. QE-6, 725 (1970).
[21] R. H. Picard and P. Schweitzer, Phys. Rev. A, 1, 1803 (1970).
[22] H. P. Weber, Phys. Lett. **27A**, 321 (1968).
[23] H. E. Rowe and T. Li, IEEE J. Quantum Electron. QE-6, 49 (1970).
[24] D. Von der Linde, IEEE J. Quantum Electron. QE-8, 328 (1972).
[25] M. A. Duguay, J. A. Giordmaine, and S. L. Shapiro, Appl. Phys. Lett. **13**, 174 (1968).
[26] C. Chen and J. M. Liu, Appl. Phys. Lett. 47, 662-664 (1985).
[27] G. P. Agrawal, *Nonlinear* Fiber *Optics* (Academic Press, New York 1989).